Autonomous artificial nanomotor powered by sunlight

Vincenzo Balzani[†‡], Miguel Clemente-León[†§], Alberto Credi[†‡], Belén Ferrer[†¶], Margherita Venturi[†], Amar H. Flood[‖], and J. Fraser Stoddart[‡‖]

[†]Dipartimento di Chimica ''G. Ciamician,'' Università di Bologna, via Selmi 2, 40126 Bologna, Italy; and [‖]California NanoSystems Institute and Department of Chemistry and Biochemistry, 405 Hilgard Avenue, University of California, Los Angeles, CA 90095

Edited by Jack Halpern, University of Chicago, Chicago, IL, and approved December 6, 2005 (received for review October 14, 2005)

Light excitation powers the reversible shuttling movement of the ring component of a rotaxane between two stations located at a 1.3-nm distance on its dumbbell-shaped component. The photoinduced shuttling movement, which occurs in solution, is based on a ''four-stroke'' synchronized sequence of electronic and nuclear processes. At room temperature the deactivation time of the high-energy charge-transfer state obtained by light excitation is ≈10 μs, and the time period required for the ring-displacement process is on the order of 100 μs. The rotaxane behaves as an autonomous linear motor and operates with a quantum efficiency up to ≈12%. The investigated system is a unique example of an artificial linear nanomotor because it gathers together the following features: (*i*) it is powered by visible light (e.g., sunlight); (*ii*) it exhibits autonomous behavior, like motor proteins; (*iii*) it does not generate waste products; (*iv*) its operation can rely only on intramolecular processes, allowing in principle operation at the single-molecule level; (*v*) it can be driven at a frequency of 1 kHz; (*vi*) it works in mild environmental conditions (i.e., fluid solution at ambient temperature); and (*vii*) it is stable for at least 10^3 cycles.

molecular machine | nanoscience | photochemistry | rotaxane | supramolecular chemistry

The miniaturization race is encouraging scientists to design and construct motors on the nanometer scale, that is, at the molecular level (1–5). Such a daring goal finds its scientific origin in the existence of natural molecular motors (6–9).

Natural molecular motors, however, are extremely complex, and any attempt to construct systems of such a complexity, using the bottom-up molecular approach (10), would be challenging. What can be done, at present, is to construct simple prototypes of artificial molecular motors and machines (1–5, 11–19), consisting of a few components capable of moving in a controllable way, and to investigate the associated problems posed by interfacing them with the macroscopic world (20–25), particularly as far as energy supply is concerned.

Natural motors are ''autonomous'': they keep operating, in a constant environment, as long as the energy source is available. By contrast, apart from a few recent examples (26–28), the fuel-powered artificial motors described so far are not autonomous because, after the mechanical movement induced by a chemical input, they need another, opposite chemical input to reset, which also implies generation of waste products. Addition of a fuel, however, is not the only means by which energy can be supplied to a chemical system. In fact, nature shows that, in green plants, the energy needed to sustain the machinery of life is ultimately provided by sunlight. Energy inputs in the form of photons can indeed cause mechanical movements by reversible chemical reactions without formation of waste products (13, 14, 16, 17).

In a previous work (29), we reported on the rotaxane $\mathbf{1}^{6+}$ (Scheme 1) that was carefully designed and synthesized to perform as a linear molecular motor powered exclusively by visible light, with autonomous operation relying on intramolecular processes. In such a work, however, we only succeeded in demonstrating the operation of the rotaxane as a light-driven mechanical switch that needed alternate addition of two ''fuels,''

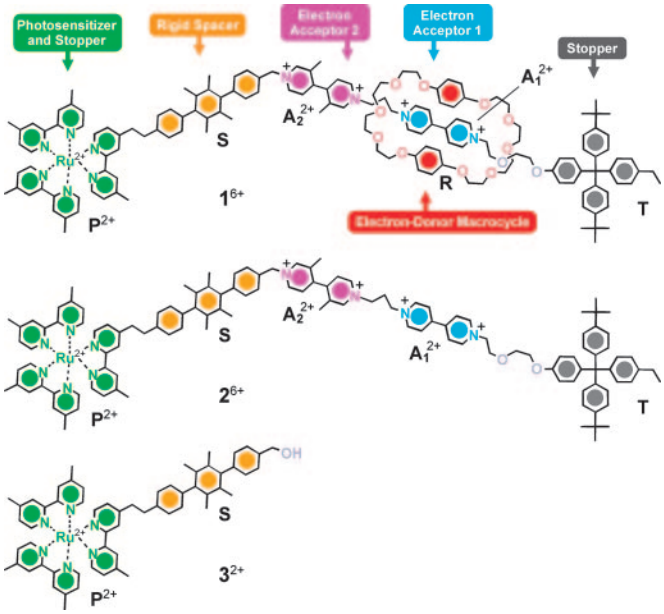

Scheme 1. Structural formulas of rotaxane $\mathbf{1}^{6+}$, its dumbbell-shaped component $\mathbf{2}^{6+}$, and model compound $\mathbf{3}^{2+}$.

namely triethanolamine and oxygen, with concomitant generation of waste products. In this work, we show that $\mathbf{1}^{6+}$ does behave as an autonomous ''four stroke'' motor powered only by sunlight, without generation of waste products. We have measured the rate constants and the efficiencies of the electronic and nuclear processes on which the shuttling movement is based, and we also discuss the related energetic aspects.

Just like their macroscopic counterparts, molecular-level machines have to be organized structurally and work as functionally integrated multicomponent systems (1). The rotaxane $\mathbf{1}^{6+}$ consists of as many as six molecular components suitably chosen and assembled to achieve the devised function. It comprises a bis-*p*-phenylene-34-crown-10 electron donor macrocycle **R** (hereafter called the ring) and a dumbbell-shaped component that contains two electron acceptor recognition sites for the ring, namely a 4,4′-bipyridinium ($\mathbf{A_1}^{2+}$) and a 3,3′-dimethyl-4,4′-bipyridinium ($\mathbf{A_2}^{2+}$) units, that can play the role of ''stations'' for the ring **R**. Molecular modeling shows that the overall length of $\mathbf{1}^{6+}$ is ≈5 nm and the distance between the centers of the two

Conflict of interest statement: No conflicts declared.

This paper was submitted directly (Track II) to the PNAS office.

Abbreviation: SCE, saturated calomel electrode.

[‡]To whom correspondence may be addressed. E-mail: vincenzo.balzani@unibo.it, alberto.credi@unibo.it, or stoddart@chem.ucla.edu.

[§]Present address: Instituto de Ciencia Molecular, Universidad de Valencia, Dr. Moliner 20, 46100 Burjassot, Spain.

[¶]Present address: Departamento de Química, Universidad Politécnica de Valencia, Camino de Vera s/n, 46022 Valencia, Spain.

www.pnas.org/cgi/doi/10.1073/pnas.0509011103

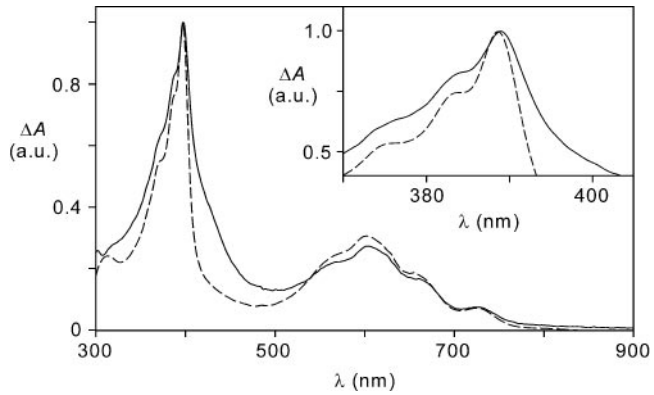

Fig. 1. UV-visible difference absorption spectra obtained upon electrochemical reduction of $\mathbf{1}^{6+}$ (solid line) and $\mathbf{2}^{6+}$ (dashed line) at −0.50 V vs. SCE in a spectroelectrochemical thin-layer cell (5.0×10^{-4} mol·liter^{-1} acetonitrile solution at room temperature). The spectra were normalized to the intense band peaking at 392 nm for $\mathbf{1}^{6+}$. (*Inset*) Detail of the spectra in the 370–405 nm region.

stations, measured along the dumbbell, is ≈1.3 nm. Furthermore, the dumbbell-shaped component incorporates a $[Ru(bpy)_3]^{2+}$-type (bpy, 2,2′-bipyridine) electron transfer photosensitizer $\mathbf{P}^{2+}$ that is able to operate with visible light and also plays the role of a stopper, a *p*-terphenyl-type rigid spacer **S** that has the task of keeping the photosensitizer far from the electron acceptor units, and finally a tetraarylmethane group **T** as the second stopper, crucial for the template-directed slippage synthesis of the rotaxane $\mathbf{1}^{6+}$ from the ring **R** and its dumbbell-shaped precursor $\mathbf{2}^{6+}$.

Results and Discussion

Electrochemical Switching. Electrochemical and NMR spectroscopic data showed (29) that the stable conformation of $\mathbf{1}^{6+}$ is by far the one in which the **R** component is located around the better electron acceptor station, $\mathbf{A}_1^{2+}$, as represented in Scheme 1. When the interaction between **R** and $\mathbf{A}_1^{2+}$ is switched off by selective reduction of $\mathbf{A}_1^{2+}$ to $\mathbf{A}_1^{+}$ (−0.44 V vs. saturated calomel electrode; SCE), the ring **R** moves by Brownian motion (9, 18) to the alternative $\mathbf{A}_2^{2+}$ station. Successive oxidation restores the electron acceptor power of the $\mathbf{A}_1^{2+}$ station and therefore the ring **R** moves back again by Brownian motion to surround this station.

We have carried out in acetonitrile solution spectroelectrochemical experiments by exhaustive one-electron reduction of $\mathbf{1}^{6+}$ and $\mathbf{2}^{6+}$ at a potential of −0.50 V vs. SCE. The spectra so obtained (Fig. 1) display the characteristic absorption bands, at ≈390 and 600 nm, of the one-electron reduced form of 4,4′-bipyridinium ($\mathbf{A}_1^{+}$) moiety. There is no evidence for the formation of the one-electron reduced form of 3,3′-dimethyl-4,4′-bipyridinium ($\mathbf{A}_2^{+}$), which has a substantially different absorption spectrum.

Photochemical Switching. The $[Ru(bpy)_3]^{2+}$-type unit $\mathbf{P}^{2+}$ (Scheme 1) is capable of playing the role of a photosensitizer for ring shuttling because visible light excitation leads to the formation of a long-lived strongly reducing excited state. Except for luminescence quantum yield and lifetime (see below), the photophysical and electrochemical properties of the photosensitizer $\mathbf{P}^{2+}$ unit contained in $\mathbf{1}^{6+}$ and $\mathbf{2}^{6+}$ are the same as those exhibited by the model compound $\mathbf{3}^{2+}$: absorption, λ_{max} = 458 nm, ε_{max} = 14,800 liters·mol^{-1}·cm^{-1}; emission, λ_{max} = 618 nm, τ = 880 ns; Φ_{em} = 0.065; excited-state energy ≈2.1 eV (1 eV = 1.602×10^{-19} J); $E_{1/2}(\mathbf{P}^{2+}/\mathbf{P}^{+})$ = +1.15 V vs. SCE. It is worthwhile recalling that the $\mathbf{P}^{2+}$ unit can harvest sunlight quite efficiently because it displays a broad and intense absorption band in the visible region.

The overall mechanism devised to perform the light-driven shuttling process in the rotaxane $\mathbf{1}^{6+}$ is based on the following four phases (Scheme 2*a*).

(a) Destabilization of the stable conformation. Light excitation of the photoactive unit $\mathbf{P}^{2+}$ (step 1) is followed by the transfer of an electron from the $^*\mathbf{P}^{2+}$ excited state to the $\mathbf{A}_1^{2+}$ station, which is encircled by the ring **R** (step 2), with the consequent "deactivation" of this station; such a photoinduced electron-transfer process has to compete with the intrinsic decay of $^*\mathbf{P}^{2+}$ (step 3).

(b) Ring displacement. After reduction ("deactivation") of the $\mathbf{A}_1^{2+}$ station to $\mathbf{A}_1^{+}$, the ring moves by Brownian motion to $\mathbf{A}_2^{2+}$ (step 4), a step that has to compete with back electron-transfer from $\mathbf{A}_1^{+}$ to the oxidized photoactive unit $\mathbf{P}^{3+}$ (step 5). This requirement is the most difficult one to meet because step 4 involves only slightly exergonic nuclear motions, whereas step 5 is an exergonic outer-sphere electron transfer process.

(c) Electronic reset. A back electron-transfer process from the "free" reduced station $\mathbf{A}_1^{+}$ to $\mathbf{P}^{3+}$ (step 6) restores the electron acceptor power of the $\mathbf{A}_1^{2+}$ station.

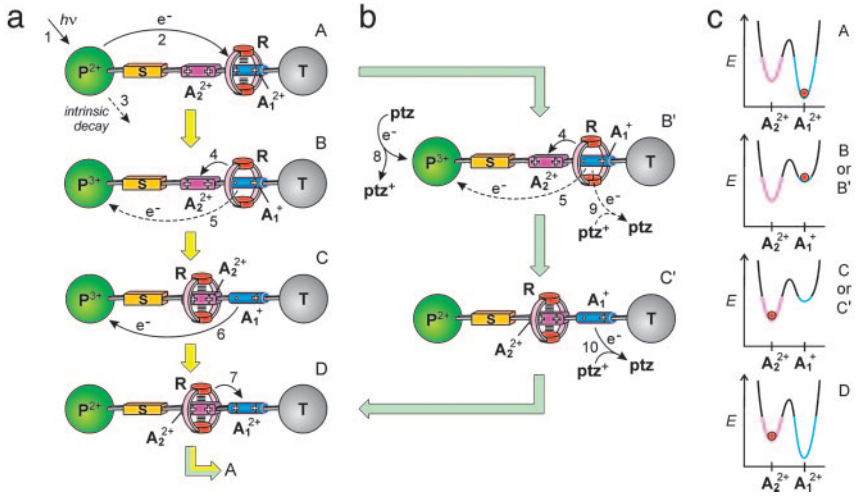

Scheme 2. Mechanisms of the photochemically driven ring shuttling in $\mathbf{1}^{6+}$. (*a*) Intramolecular mechanism. (*b*) Shuttling assisted by an electron relay. (*c*) Graphical representation of how the energy profile of shuttling changes upon reduction of $\mathbf{A}_1^{2+}$ and the location of the ring at $\mathbf{A}_1^{2+}$ (blue) or $\mathbf{A}_2^{2+}$ (magenta) for each molecular structure illustrated.

Table 1. Kinetic data for photoinduced processes of 1^{6+} in deaerated acetonitrile solution in the temperature range 284–303 K

T, K	k_{et}, s^{-1}	k_{bet}, s^{-1}	k_{ptz}, liter·mol^{-1}·s^{-1}	k_{rd}, s^{-1}	τ_{bet}, μs	τ_{rd}, μs
284	1.5×10^5 (1.8×10^5)	1.4×10^5 (5.4×10^5)	7.9×10^8 (5.0×10^8)	8.1×10^2	7.4 (1.8)	1,230
288	1.7×10^5 (2.0×10^5)	1.4×10^5 (5.9×10^5)	8.4×10^8 (5.0×10^8)	1.8×10^3	7.1 (1.7)	550
293	1.7×10^5 (2.1×10^5)	1.4×10^5 (6.7×10^5)	7.6×10^8 (4.9×10^8)	3.5×10^3	7.0 (1.5)	285
299	1.8×10^5 (2.4×10^5)	1.4×10^5 (7.0×10^5)	7.8×10^8 (4.8×10^8)	1.3×10^4	7.1 (1.4)	78
303	2.5×10^5 (3.1×10^5)	1.5×10^5 (6.9×10^5)	8.1×10^8 (4.8×10^8)	2.1×10^4	6.7 (1.4)	47

The corresponding data for 2^{6+} are reported in parentheses. Subscripts are defined as follows: et, photoinduced electron transfer (Scheme 2*a*, step 2); bet, back electron transfer (Scheme 2*a*, steps 5 and 6); ptz, bimolecular electron transfer between the A_1^+ unit and **ptz**$^+$ (Scheme 2*b*, steps 9 and 10); rd, displacement of the ring from A_1^+ to the A_2^{2+} station corresponding to the shift of the transient absorption maximum of the A_1^+ unit (Scheme 2 *a* and *b*, step 4).

(d) Nuclear reset. As a consequence of the electronic reset, the ring moves back again by Brownian motion from A_2^{2+} to A_1^{2+} (step 7).

To verify whether such a devised mechanism works, we have performed luminescence quenching and flash photolysis experiments both in the absence and presence of phenothiazine as an electron relay.

Luminescence quenching. In deaerated acetonitrile solution containing the rotaxane 1^{6+} or the dumbbell-shaped compound 2^{6+}, the emission lifetimes and intensities of the P^{2+} units are quenched when compared with the values obtained for the model compound 3^{2+}. The occurrence of dynamic quenching can be ruled out because of the high dilution of the solution. As will be clear from the transient absorption data, the luminescence quenching is due to an electron-transfer process from the $^*P^{2+}$ excited state to the A_1^{2+} unit. The luminescence lifetimes and quantum yields for the electron transfer process at different temperatures are gathered in Table 3, which is published as supporting information on the PNAS web site. The values for the electron transfer rate constant k_{et} are reported in Table 1.

Flash photolysis. Upon flash excitation of 1^{6+}, transient absorption spectral changes were observed (see Fig. 5, which is published as supporting information on the PNAS web site). The transient spectrum 6 μs after light excitation displayed the features of the monoreduced 4,4′-bipyridinium unit A_1^+ (for the monoreduced form of the 1,1′-dibenzyl-4,4′-bipyridinium model compound in acetonitrile, $\lambda_{max} = 402$ nm and $\varepsilon_{max} = 35{,}000$ liters·mol^{-1}·cm^{-1}) and some residual bleaching in the spectral region of the ground state absorption of P^{2+}. There is no evidence of formation of the monoreduced 3,3′-dimethyl-4,4′-bipyridinium unit, A_2^+, whose spectrum is substantially different from that of A_1^+. These results indicate that the species formed upon light excitation of 1^{6+} is a compound in which an electron has been transferred from the $^*P^{2+}$ excited state to the A_1^{2+} unit. The same results have been obtained for dumbbell 2^{6+}.

In the case of model compound 3^{2+}, where photoinduced electron transfer cannot take place because it does not contain any electron acceptor unit, the observed spectral changes were consistent with the formation of the excited state of the P^{2+} unit (see Fig. 6, which is published as supporting information on the PNAS web site). The decay time of the transient absorption spectrum was in full agreement with the luminescence decay. An isosbestic point between the absorption spectra of the ground and excited states of the P^{2+} unit in such a model compound was found at $\lambda_{iso} = 398$ nm. This observation and the fact that the spectrum of A_1^+ possesses a very intense band peaking in the same region (Fig. 1) allowed us to monitor the formation and decay of the A_1^+ unit in the case of 1^{6+} and 2^{6+}, and hence to measure the rate constants for the forward ($^*P^{2+}$ to A_1^{2+}, step 2; Scheme 2*a*) and the back (A_1^+ to P^{3+}, steps 5 and 6; see below) electron transfer processes. Typical transient absorption kinetics recorded at λ_{iso} are shown in Fig. 7, which is published as supporting information on the PNAS web site.

The changes of the transient absorption, monitored at λ_{iso}, as a function of time were measured at five different temperatures (the exact position of λ_{iso} was determined on model compound 3^{2+} at each temperature). In all cases, the rise time of the transient absorption was in agreement, within experimental error, with the lifetime of the excited state of the P^{2+} component (Table 3), and the transient absorption signal completely disappeared with the first-order rate constants, k_{bet} reported in Table 1. We have also observed that both 1^{6+} and 2^{6+} do not undergo any photodegradation after 10^3 light pulses. The quantum yields of the photoinduced electron transfer processes obtained from transient absorption data are in agreement, within experimental error, with those found from luminescence measurements.

In summary, the luminescence and transient absorption data demonstrate that visible excitation of the P^{2+} component in 1^{6+} and 2^{6+} causes an electron transfer process (k_{et}) to the A_1^{2+} unit, followed by a back electron transfer (k_{bet}) leading to the ground state according to a monoexponential law (Table 2).

In the rotaxane 1^{6+} the back electron transfer can take place by either step 5 or 6 (Scheme 2*a*), depending on the rate of ring displacement (step 4). If step 5 is much faster than step 4, the photoinduced electron transfer is simply followed by a back

Table 2. Values of the efficiency of ring displacement, η_{rd}, and quantum yield of ring shuttling, Φ_{sh}, for 1^{6+} in the temperature range 284–303 K

		Intramolecular mechanism (Scheme 2*a*)			Mechanism with assistance of phenothiazine (Scheme 2*b*)		
T, K	k_4, s^{-1}	k_5, s^{-1}	η_{rd}	Φ_{sh}	k_9[**ptz**$^+$]$_0$, s^{-1}	η_{rd}	Φ_{sh}
284	8.1×10^2	1.4×10^5	<0.01	<0.001	2.5×10^3	0.25	0.04
288	1.8×10^3	1.4×10^5	0.01	0.002	3.2×10^3	0.36	0.06
293	3.5×10^3	1.4×10^5	0.025	0.004	3.3×10^3	0.51	0.08
299	1.3×10^4	1.3×10^5	0.09	0.015	5.1×10^3	0.72	0.12
303	2.1×10^4	1.3×10^5	0.14	0.02	6.7×10^3	0.76	0.12

Conditions were as follows: deaerated acetonitrile solution, and, for the assisted mechanism of Scheme 2*b*, [**ptz**] $= 5.0 \times 10^{-5}$ mol·liter^{-1}.

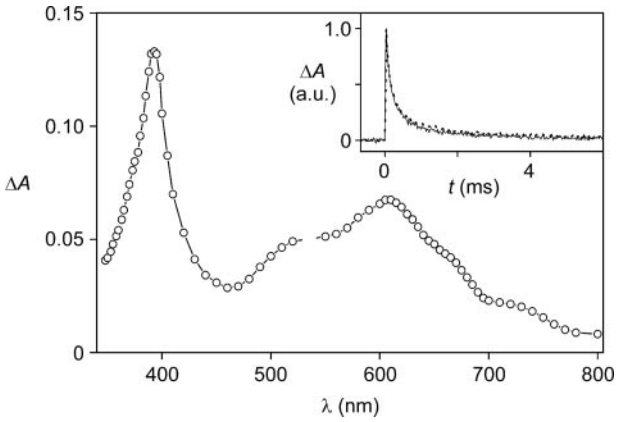

Fig. 2. Transient UV-visible absorption difference spectrum of a deaerated acetonitrile solution containing 1.0×10^{-4} mol·liter^{-1} $\mathbf{1}^{6+}$ and 5.0×10^{-5} mol·liter^{-1} **ptz**, recorded 50 μs after 532-nm laser excitation at room temperature. (*Inset*) Normalized transient absorption decays monitored at 520 (solid line) and 600 (dotted line) nm, which correspond to signals assigned to $\mathbf{ptz}^+$ and $\mathbf{A_1}^+$, respectively.

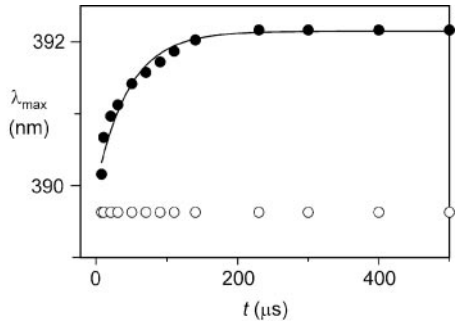

Fig. 3. Time dependence of the wavelength of the absorption maximum (λ_{max}) of the UV band of photogenerated $\mathbf{A_1}^+$ for $\mathbf{1}^{6+}$ (filled circles) and $\mathbf{2}^{6+}$ (open circles) at 303 K. The full line represents the monoexponential data fit used to obtain k_{rd} for $\mathbf{1}^{6+}$.

electron transfer, without any ring motion. If, on the contrary, step 4 is much faster than step 5, the photoinduced electron transfer causes the displacement of the ring **R** from the $\mathbf{A_1}^+$ station to $\mathbf{A_2}^{2+}$. In such a case, back electron transfer (now step 6) leads subsequently to the unstable isomer of $\mathbf{1}^{6+}$ (D in Scheme 2*a*) which relaxes thermally (step 7) to give back the starting conformation. If the rates of steps 4 and 5 are not much different from each other, both steps 5 and 6 contribute to the back electron transfer process. The results discussed above showed that steps 1, 2, 3, and 5 and/or 6 take place, but we were not able to establish whether the photoinduced ring displacement, step 4, occurs (Scheme 2*a*). This problem has been tackled as discussed below.

Experiments in the presence of phenothiazine as an electron relay. We have used an electron relay to slow down the back electron transfer process (step 5) to observe the ring displacement (step 4) and measure its rate.

A compound **X** capable of playing the role of an electron relay in our system must satisfy several requirements: (*i*) it should not quench the $^*\mathbf{P}^{2+}$ excited state by energy transfer; (*ii*) its oxidation process must be chemically reversible; (*iii*) its $\mathbf{X}^+/\mathbf{X}$ redox potential must be less positive than that of $\mathbf{P}^{3+}/\mathbf{P}^{2+}$ (+1.15 V vs. SCE) to scavenge $\mathbf{P}^{3+}$; and (*iv*) both **X** and $\mathbf{X}^+$ should not absorb the light used to cause the photoreaction and to monitor its occurrence. After trying and discarding several compounds (DABCO, diphenylamine and triphenylamine), we chose phenothiazine, **ptz,** which is reversibly oxidized [$E_{1/2}(\mathbf{ptz}^+/\mathbf{ptz})$ = +0.60 V vs. SCE] (30) and does not show absorption bands in the visible region. Furthermore, its radical cation $\mathbf{ptz}^+$ exhibits a band at 520 nm (31) that does not interfere with the spectrum of $\mathbf{A_1}^+$ and also can be useful for monitoring the behavior of the electron relay during the process.

When photoexcitation of $\mathbf{1}^{6+}$ is performed in the presence of **ptz** (Scheme 2*b*), the photoinduced electron transfer (step 2) is expected to be followed by a diffusion-controlled reaction between **ptz** and $\mathbf{P}^{3+}$ with formation of $\mathbf{ptz}^+$ and regeneration of $\mathbf{P}^{2+}$ (step 8). Therefore, intramolecular back electron transfer (step 5) should no longer occur, and ring displacement (step 4) should successfully compete with the much slower intermolecular back electron transfer reaction between $\mathbf{ptz}^+$ and $\mathbf{A_1}^+$ (step 9).

Flash-photolysis experiments of solutions containing $\mathbf{1}^{6+}$ or $\mathbf{2}^{6+}$ (1.0×10^{-4} mol·liter^{-1}) and phenothiazine (5.0×10^{-5} mol·liter^{-1}) at all of the examined temperatures showed the presence of the characteristic bands of $\mathbf{A_1}^+$ at ≈390 and 600 nm and of $\mathbf{ptz}^+$ at 520 nm (Fig. 2). The transient absorption signals at 600, 520, and 390 nm completely disappeared according to identical second-order processes occurring in the millisecond time scale (Table 1 and Fig. 2 *Inset*). Therefore, under such conditions the back electron transfer reaction is much slower (from 2 to 3 orders of magnitude) than in the absence of **ptz,** thereby leaving more time for ring displacement.

To measure the rate of ring displacement, we carefully analyzed the time evolution of the shape of the 390-nm transient absorption band of the reduced station $\mathbf{A_1}^+$ (see *Supporting Text* and Figs. 8–10, which are published as supporting information on the PNAS web site). We found that the maximum of such a band in $\mathbf{1}^{5+}$ undergoes a slight red shift upon decay, whereas it does not change for $\mathbf{2}^{5+}$ (Fig. 3), which has the same structural elements of the rotaxane, except for the "movable" ring, and features all of the processes that allow the operation of the motor but the motion of the ring itself. The shift of the maximum of the $\mathbf{A_1}^+$ band in $\mathbf{1}^{5+}$ that accompanies the transient signal decay thus can be related to the displacement of the ring from $\mathbf{A_1}^+$ to $\mathbf{A_2}^{2+}$ ($k_{rd,}$ step 4 in Scheme 2*a*). This assumption is supported by the fact that, 850 μs after light excitation (303 K), the transient UV band in the case of $\mathbf{1}^{6+}$ is slightly red-shifted compared with that observed for $\mathbf{2}^{6+}$ (Fig. 3) as observed in the spectroelectrochemical experiments between the one electron reduced form $\mathbf{1}^{5+}$ (in which the ring encircles $\mathbf{A_2}^{2+}$) and $\mathbf{2}^{5+}$ (Fig. 1).

A kinetic analysis (see ref. 14 and *Supporting Text*) has shown that the shift of the band maximum (i.e., the ring displacement) takes place according to a monoexponential law (Fig. 3) with a rate constant, k_{rd}, that rises with increasing temperature (Table 1; see also Fig. 11, which is published as supporting information on the PNAS web site). The free energy of activation for the ring displacement is ≈50 kJ·mol^{-1} at 298 K. The relatively small values of the ring displacement rate constants suggest that such a movement requires considerable structural rearrangements, possibly including unfolding processes. Under the experimental conditions used, both $\mathbf{1}^{6+}$ or $\mathbf{2}^{6+}$ showed a reversible behavior, with no change in the steady-state absorption and luminescence spectra after 10^3 laser pulses.

In conclusion, in the presence of **ptz** the photoinduced electron transfer reaction (step 2) is unaffected (for more details, see *Supporting Text*; see also Fig. 12, which is published as supporting information on the PNAS web site), $\mathbf{P}^{3+}$ is completely scavenged by **ptz** (step 8), ring displacement takes place (step 4), and both electron (steps 9 and/or 10) and nuclear (step 7) reset processes occur quantitatively because the system can undergo at least 10^3 cycles. Therefore $\mathbf{1}^{6+}$ behaves as an autonomous molecular motor that consumes only photons of visible light (Scheme 2*b*). The role played by **ptz** is that of an electron relay with a "negative" kinetic effect.

Intramolecular mechanism. As reported above, by using **ptz** as an electron relay we have obtained the rate (k_{rd}; Table 2) of ring displacement (step 4) from the photogenerated $\mathbf{A_1^+}$ station to the $\mathbf{A_2^{2+}}$ station. Therefore, we can go back to the discussion about what happens in the absence of **ptz** (Scheme 2*a*). To understand whether ring displacement takes place also in the case of the intramolecular mechanism, we must compare the values of k_4 (i.e., k_{rd}) and k_5, the rate of the back electron-transfer process from the $\mathbf{A_1^+}$ station, still encircled by the ring, to $\mathbf{P}^{3+}$. The kinetic treatment and more details are given in *Supporting Text* and Schemes 3 and 4, which are published as supporting information on the PNAS web site. Contrary to what happens when **ptz** is present, in the case of the intramolecular mechanism the exact position of $\mathbf{A_1^+}$ absorption maximum and, if any, its shift during the signal decay cannot be established because of interference by the absorption spectra of $^*\mathbf{P}^{2+}$ and $\mathbf{P}^{3+}$. However, we can estimate the rate constant of step 6 from the experiments performed on the dumbbell component $\mathbf{2}^{6+}$ ($k_{bet} = k_6$), and we can reasonably assume that k_{rd} is the same as that observed for the **ptz**-assisted mechanism. From Table 2 we can see that k_6 (i.e., k_{bet} for $\mathbf{2}^{6+}$) is at least 35 times larger than k_{rd}, so that conformer C has to disappear (step 6) as soon as it is formed (step 4). Therefore, in $\mathbf{1}^{6+}$ $k_{bet} = k_5 + k_{rd}$. At 303 K (Table 1) $k_5 = 1.5 \times 10^5 - 2.1 \times 10^4 = 1.3 \times 10^5\ s^{-1}$, which means that the displacement of the ring (step 4) competes (14%) with the intramolecular back electron transfer (step 5, Scheme 2*a*). In conclusion, also in the absence of **ptz** the shuttling process does take place with appreciable efficiency at 303 K. The drawback of the low efficiency is compensated by the fact that the operation of the system relies exclusively on intramolecular processes. This artificial molecular motor does not rely on consumption or even assistance of external species; it is stable for at least 10^3 cycles, and it operates by simply exposing the solution to sunlight.

Shuttling Efficiency. As we have seen above, the results obtained have allowed us to establish the following relationship among the rate constants of the steps involved in the intramolecular and **ptz**-assisted mechanisms (Scheme 2) and the experimentally determined rate constants (Tables 1–3): $k_2 = k_{et}$ (Table 2); $k_3 = 1/\tau_0$ (Table 1); $k_4 = k_{rd}$ (Table 2); $k_5 = k_{bet} - k_{rd}$ (Table 3); k_6 and k_{10} are obtained from the experimentally measured k_{bet} of $\mathbf{2}^{6+}$ (Table 1); k_9 is obtained from Eq. **S13** in *Supporting Text* (Table 2, in which the values of $k_9[\mathbf{ptz}^+]_0$, more easily comparable with k_4, are reported). Concerning step 8, its rate constant is diffusion controlled, $k_8 \approx 1 \times 10^{10}$ liters·mol^{-1}·s^{-1}, and under our experimental conditions it is fast enough to fully prevent intramolecular back electron transfer, thereby activating the sequence of processes illustrated in Scheme 2*b*. Finally, step 7 is thermodynamically allowed, and it does not compete with any other step; the value of its rate constant, k_7, which is not relevant for the discussion on quantum yields and efficiencies, is estimated to be $10^3\ s^{-1}$ (see *Supporting Text*).

We can now discuss the performance of $\mathbf{1}^{6+}$ as a photochemically driven molecular motor when it operates according to the mechanisms illustrated in Scheme 2. The quantum yield of the shuttling process (number of ring shuttling events divided by number of absorbed photons) amounts to $\Phi_{sh} = \Phi_{et} \times \eta_{rd} \times \eta_{er} \times \eta_{nr}$, where Φ_{et} is the quantum yield of the photoinduced electron transfer process that causes the destabilization of the stable conformation A, η_{rd} is the efficiency of ring displacement, η_{er} is the efficiency of the electronic reset, and η_{nr} is the efficiency of the nuclear reset.

The quantum yield of the photoinduced electron transfer process is the same, regardless of the working mechanism, $\Phi_{et} = k_2/(k_2+k_3)$, e.g., 0.16 at 303 K (Scheme 2 and Table 3). The efficiency of the electronic reset, η_{er}, is equal to unity in both mechanisms because back electron transfer takes place in any case (via steps 5 and 6 in the intramolecular mechanism and via steps 9 and 10 in the **ptz**-assisted one), as shown by lack of any degradation after 10^3 cycles. The efficiency of the nuclear reset, η_{nr}, is equal to 1 in all cases because k_7 does not compete with any other step. Therefore, the expression of the quantum yield of ring shuttling reduces to $\Phi_{sh} = \Phi_{et} \times \eta_{rd}$. The efficiency η_{rd} depends on the operating mechanism and the experimental conditions, as shown in Table 2. The values of Φ_{sh} at the various temperatures examined also are gathered in Table 2.

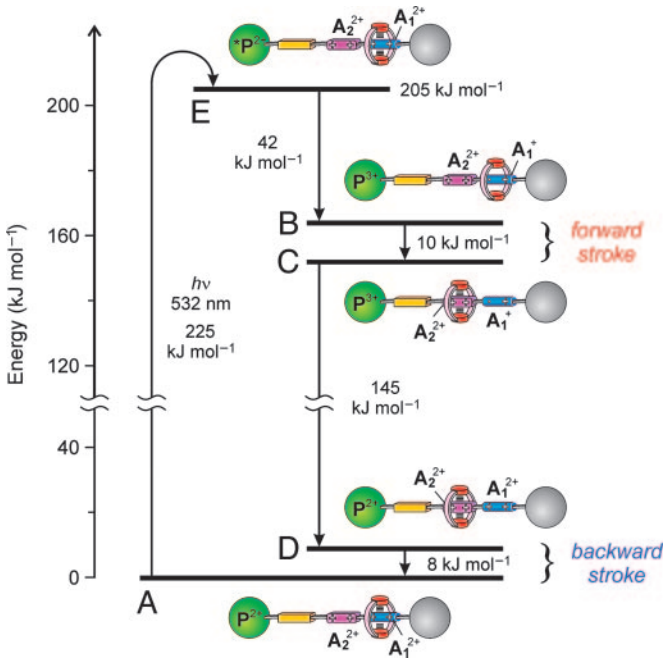

Fig. 4. Energy level diagram for the processes taking place in rotaxane $\mathbf{1}^{6+}$ when it works as a light-driven molecular motor based on intramolecular processes at room temperature (see Scheme 2*a*). The energy of a 532-nm photon (225 kJ·mol^{-1}) is used to produce the long-lived excited state of the $\mathbf{P}^{2+}$ component (205 kJ·mol^{-1}, E), which decays by electron transfer to the $\mathbf{A_1^{2+}}$ station (B) with 14% yield. An energy of 10 kJ·mol^{-1} is then released in the Brownian motion of the ring R over the 50 kJ·mol^{-1} barrier (forward stroke) from $\mathbf{A_1^+}$ to $\mathbf{A_2^{2+}}$ (C). A further 145 kJ·mol^{-1} is used to transfer the electron from $\mathbf{A_1^+}$ back to $\mathbf{P}^{3+}$ (D), and the remaining 8 kJ·mol^{-1} is released in the motion of the ring (backward stroke) from $\mathbf{A_2^{2+}}$ to $\mathbf{A_1^{2+}}$ (A).

When $\mathbf{1}^{6+}$ works according to the intramolecular mechanism (Scheme 2*a*), at 303 K $\eta_{rd} = 0.14$, and therefore the quantum yield for the shuttling process, Φ_{sh}, is ≈2%. On decreasing temperature, the quantum yield decreases because k_4 (i.e., k_{rd}) refers to a strongly activated process, whereas $(k_5 + k_4)$ (i.e., k_{bet}) is almost temperature independent.

When $\mathbf{1}^{6+}$ works with assistance of **ptz** (Scheme 2*b*), at 303 K $\eta_{rd} = 0.76$ and $\Phi_{sh} = 12\%$. On decreasing temperature η_{rd} decreases, but Φ_{sh} is still appreciable (4%) at 284 K. On changing the $\mathbf{ptz}^+$ concentration, the values of η_{rd} and Φ_{sh} would of course change.

Energetics. The energy available (ΔG°_T) for the shuttling, which could, in principle, be used to do mechanical work, can be estimated on the basis of thermodynamic considerations (see Scheme 5, which is published as supporting information on the PNAS web site). The energy levels involved in the photoinduced ring shuttling of $\mathbf{1}^{6+}$ at room temperature are shown in Fig. 4. Altogether, the fraction F of the excited-state energy used for the motion of the ring amounts to ≈10%, and the overall efficiency of light-to-mechanical energy conversion, $\eta_{en.conv.} = \Phi_{sh} \times F$, is ≈1% for the kinetically assisted system and ≈0.2% in the case of the intramolecular mechanism (at 303 K). Considering that the nuclear reset (step 7 in Scheme 2*a*) is 1 ms, the motor can be

driven at a frequency of 10^3 Hz, potentially generating a power of 3×10^{-17} W per molecule.

Conclusions

We have shown that in rotaxane $\mathbf{1}^{6+}$ displacement of the ring for 1.3 nm between the two stations $\mathbf{A_1}^{2+}$ and $\mathbf{A_2}^{2+}$, that are placed along the dumbbell-shaped component, can be obtained by light energy inputs without consumption of chemical fuels and formation of waste products. Such photoinduced ring displacement can occur by (*i*) a purely intramolecular mechanism and (*ii*) an intermolecular mechanism, involving the assistance of an external electron relay. The system behaves as an autonomous linear motor powered by visible light, and its operation takes place in four strokes: destabilization of the stable conformation, displacement of the ring, electronic reset, and nuclear reset.

Each phase (Scheme 2*a*) corresponds, in kind, to the fuel injection and combustion (A), piston displacement (B), exhaust removal (C), and piston replacement (D) of a four-stroke engine. The timing of the strokes is intrinsic to the molecular motor and cannot be tuned up externally as in fuel-injected car engines. The mechanism relies indeed on the competition between the motion of the ring (step 4) and the back electron transfer (step 5). If the latter process is much faster than the former, the photoinduced electron transfer (step 2) is simply followed by a back electron transfer (step 5), with no relative motion involving the ring. Such a situation would be equivalent to injection of fuel and removal before combustion. In the present case, at 303 K, the back electron transfer is 7 times faster than ring displacement, leading to an overall quantum efficiency of the motor of 2%. When the ring shuttling is assisted by the electron relay (Scheme 2*b*), the "negative" kinetic effect exerted by **ptz** on the back electron transfer increases the overall quantum efficiency of the motor to 12%.

The low efficiency of this motor when it works in an autonomous way with the assistance of an external relay, and even more so when it works purely with an intramolecular mechanism, may seem disappointing, but it should be noted that the fuel (sunlight) is free. Besides being powered by sunlight and operating as an autonomous motor, the investigated system shows other quite interesting properties: it works in mild environmental conditions, it is remarkably stable, and it can be driven at high frequency (kilohertz). In principle, when working by intramolecular mechanism, it is also suitable for operation at the single-molecule level.

The field of artificial molecular motors is still in its infancy. The construction of an autonomous, sunlight-driven molecular motor was a very ambitious task from the outset. Our results show that the structural and functional integration of suitably selected modular units into carefully designed multicomponent molecular systems is indeed a valuable approach.

Materials and Methods

The syntheses of $\mathbf{1}^{6+}$, $\mathbf{2}^{6+}$, and $\mathbf{3}^{2+}$ have been previously reported (29).

Spectroelectrochemical measurements were performed *in situ* with a custom-made optically transparent thin-layer electrochemical cell by using a diode array spectrophotometer. The working and counter electrodes were Pt minigrids, and the quasi-reference electrode was an Ag wire; all three electrodes were melt-sealed into a polyethylene spacer.

Luminescence decay and transient absorption experiments were performed in degassed acetonitrile solutions by exciting the sample with 10 ns (full width at half maximum) pulses from the second harmonic (532 nm) of a Nd:YAG laser. In the transient absorption studies, a Xe lamp perpendicular to the laser beam was used as a probing light. The absorption transient decays were plotted as $\Delta A = \log(I_0/I_t)$ vs. time, where I_0 and I_t were the probing light intensity before the laser pulse and after delay t, respectively. Transient absorption spectra were obtained from the decays measured at various wavelengths (5-nm increment), by sampling the absorbance changes at constant delay time. In the determination of the shift of λ_{max}, a wavelength increment of 1 nm in the 350–440 nm region was adopted; to obtain a significant comparison between the bands of the rotaxane and of its dumbbell-shaped component, the decay at each wavelength was measured in parallel for otherwise identical solutions of $\mathbf{1}^{6+}$ and $\mathbf{2}^{6+}$. The same laser/monochromator/phototube setup was used to measure luminescence lifetimes. The accuracy on the wavelength values was estimated to be ± 2 nm. The experimental error was 4% for the lifetime values and 20% for the quantum yield of the photoinduced electron transfer processes. More details can be found in *Supporting Text*.

We thank Dr. Lucia Flamigni for useful discussion. This work was supported by the Ministry of Education, University and Research in Italy and by the National Science Foundation. The European Union provided support under the auspices of the Biomach project and a Marie Curie Individual Fellowship (to B.F.).

1. Balzani, V., Credi, A., Raymo, F. M. & Stoddart, J. F. (2000) *Angew. Chem. Int. Ed.* **39,** 3348–3391.
2. Stoddart, J. F., ed. (2001) *Acc. Chem. Res.* **34** (6), special issue, 409–522.
3. Sauvage, J.-P., ed. (2001) *Struct. Bond.* **99,** special volume, 1–281.
4. Balzani, V., Credi, A. & Venturi, M. (2003) *Molecular Devices and Machines: A Journey into the Nano World* (Wiley-VCH, Weinheim, Germany).
5. Kelly, T. R., ed. (2005) *Top. Curr. Chem.* **262,** special volume, 1–227.
6. Schliwa, M., ed. (2002) *Molecular Motors* (Wiley-VCH, Weinheim, Germany).
7. Oster, G. & Wang, H. (2003) *Trends Cell Biol.* **13,** 114–121.
8. Goodsell, D. S. (2004) *Bionanotechnology: Lessons from Nature* (Wiley, New York).
9. Jones, R. A. L. (2005) *Soft Machines: Nanotechnology and Life* (Oxford Univ. Press, Oxford).
10. Lehn, J.-M. (2002) *Proc. Natl. Acad. Sci. USA* **99,** 4763–4768.
11. Steinberg-Yfrach, G., Rigaud, J.-L., Durantini, E. N., Moore, A. L., Gust, D. & Moore, T. A. (1998) *Nature* **392,** 479–482.
12. Kelly, T. R., De Silva, H. & Silva, R. A. (1999) *Nature* **401,** 150–152.
13. Koumura, N., Zijlstra, R. W., van Delden, R. A., Harada, N. & Feringa, B. L. (1999) *Nature* **401,** 152–155.
14. Brouwer, A. M. Frochot, C., Gatti, F. G., Leigh, D. A., Mottier, L., Paolucci, F., Roffia, S. & Wurpel, G. W. H. (2001) *Science* **291,** 2124–2128.
15. Badjic, J. D., Balzani, V., Credi, A., Silvi, S. & Stoddart, J. F. (2004) *Science* **303,** 1845–1849.
16. Hernandez, J. V., Kay, E. R. & Leigh, D. A. (2004) *Science* **306,** 1532–1537.
17. Mobian, P., Kern, J.-M. & Sauvage, J.-P. (2004) *Angew. Chem. Int. Ed.* **43,** 2392–2395.
18. Sherman, W. B. & Seeman, N. C. (2004) *Nano Lett.* **4,** 1203–1207.
19. Astumian, R. D. (2005) *Proc. Natl. Acad. Sci. USA*, **102,** 1843–1847.
20. Zheng, X. L. Mulcahy, M. E., Horinek, D., Galeotti, F., Magnera, T. F. & Michl, J. (2004) *J. Am. Chem. Soc.* **126,** 4540–4542.
21. Katz, E., Lioubashevsky, O. & Willner, I. (2004) *J. Am. Chem. Soc.* **126,** 15520–15532.
22. van Delden, R. A., ter Wiel, M. K. J., Pollard, M. M., Vicario, J., Koumura, N. & Feringa, B. L. (2005) *Nature* **437,** 1337–1340.
23. Liu, Y., Flood, A. H., Bonvallet, P. A., Vignon, S. A., Northrop, B. H., Tseng, H.-R., Jeppesen, J. O., Huang, T. J., Brough, B., Baller, M., *et al.* (2005) *J. Am. Chem. Soc.* **127,** 9745–9759.
24. Nguyen, T. D., Tseng, H.-R., Celestre, P. C., Flood, A. H., Liu, Y., Stoddart, J. F. & Zink, J. I. (2005) *Proc. Natl. Acad. Sci. USA* **102,** 10029–10034.
25. Berná, J., Leigh, D. A., Lubomska, M., Mendoza, S. M., Pérez, E. M., Rudolf, P., Teobaldi, G. & Zerbetto, F. (2005) *Nat. Mater.* **4,** 704–710.
26. Tian, Y. & Mao, C. D. (2004) *J. Am. Chem. Soc.* **126,** 11410–11411.
27. Tian, Y., He, Y., Chen, Y., Yin, P. & Mao, C. D. (2005) *Angew. Chem. Int. Ed.* **44,** 4355–4358.
28. Bath, J., Green, S. J. & Turberfield, A. J. (2005) *Angew. Chem. Int. Ed.* **44,** 4358–4361.
29. Ashton, P. R., Ballardini, R., Balzani, V., Credi, A., Dress, K. R., Ishow, E., Kleverlaan, C. J., Kocian, O., Preece, J. A., Spencer, N., *et al.* (2000) *Chem. Eur. J.* **6,** 3558–3574.
30. Kowert, B. A., Marcoux, L. & Bard, A. J. (1972) *J. Am. Chem. Soc.* **94,** 5538–5550.
31. Hanson, P. & Norman, R. O. C. (1973) *J. Chem. Soc. Perkin Trans.* **2,** 264–271.